Journal of
Applied and Computational Mechanics

Shahid Chamran University of Ahvaz

Research Paper

Vibration Mitigation of Rail Noise Barriers by Hysteretic Absorbers

Michela Basili[1], Paolo Casini[2], Laura Morelli[3], Fabrizio Vestroni[4]

[1] Department of Structural and Geotechnical Engineering, Sapienza University of Rome, Via Eudossiana 18, Rome, 00184, Italy, Email: michela.basili@uniroma1.it

[2] Department of Structural and Geotechnical Engineering, Sapienza University of Rome, Via Eudossiana 18, Rome, 00184, Italy, Email: p.casini@uniroma1.it

[3] Department of Structural and Geotechnical Engineering, Sapienza University of Rome, Via Eudossiana 18, Rome, 00184, Italy, Email: laura.morelli@uniroma1.it

[4] Department of Structural and Geotechnical Engineering, Sapienza University of Rome, Via Eudossiana 18, Rome, 00184, Italy, Email: vestroni@uniroma1.it

Abstract. A strategy is proposed to mitigate the noise barrier vibrations due to the train passage in high speed lines employing a hysteretic vibration absorber. The barrier is modelled as a generalized single degree of freedom system; the absorber consists of a light mass attached to the main structure by a hysteretic element whose restoring force is described by the Bouc-Wen model. The resulting two degrees of freedom system is studied, and it is shown that, for control purposes, beneficial conditions are obtained when the two oscillators are close to the resonance conditions (1:1). A procedure for a preliminary design of the absorber is highlighted; a parametric analysis varying the absorber characteristics is carried out and the optimal values are obtained by maximizing the barrier response performance. The absorber is realized exploiting high damping rubber elements whose constitutive parameters have been identified through experimental tests. The effectiveness of the realized absorber is assessed by performing dynamic analysis of the two degrees of freedom system under the train excitation at a reference speed and comparing its performances with those of the designed one, observing a similar reduction of the barrier response. Finally, a sensitivity analysis of the performances varying the train speed shows that, even if the stiffness and damping of the absorber are amplitude dependent, its efficiency is confirmed in the speed range of high speed trains.

Keywords: Vibrations mitigation, Hysteretic absorber, Noise barriers, Rubber elements, Experimental tests.

1. Introduction

Noise barriers are trackside structures adjacent to the railway which have the primary function of reducing the noise in the surrounding environment, as well as functioning as obstruction elements to prevent trespassing the lines. The barriers were originally designed for static actions, considering the aerodynamic pressure induced by the train transit acting as an equivalent static force. With the increase of trains speed which implies higher pressure fields and from in situ experiments, it resulted that these structures may exhibit response amplification causing weakening and fatigue problems; consequently, it becomes mandatory to consider their dynamic response and investigate possible strategies to control this phenomenon. Until the last decade, only few European countries focused on this aspect; all the evaluations were done in absence of national codes or specific requirements considering the dynamic effects induced by the train passage [1, 2]. Due to the repeated passage of trains along high speed lines, noise barriers undergo cyclic response and can be affected by fatigue phenomena, specifically, at the section of the column base, where large and alternating sign bending moments cause weakening. This aspect is intended to raise importance in the future for increasing train speeds, while only in the last years becomes a topic worthy of attention [1-6].

A part of the scientific literature on this topic is oriented to describe properly the pressure induced by the train on the barriers through field measurements [3], theoretical and experimental evaluations [4], dynamic simulations processes at different speeds [7]. Another part of the studies concerns the dynamic response of the barriers subject to the train pulse through appropriate models [2, 5, 8-11]. In particular, the resonance effect between the natural frequency of the noise barriers and the pulse excitation of the train head and tail are underlined in [5, 11]; the interaction phenomena between train and trackside structures under the aerodynamic action generated by passing trains are the subject of [8]; large finite element models are used in [9] to describe the response of barriers of existing railway bridges, taking into account different types of bridges; finally, a comparison of calculation methods for aerodynamic impact on noise barriers along high speed rail lines is given in [10]. Most of the papers emphasize the amplification of the barrier response due to train passage, however, there is lack of indication on how these vibrations could be reduced.

In the vibration mitigation, it is common to connect a structure to be protected with an attachment, which has the role of absorbing part of the vibratory energy of the excited primary structure, thus reducing its oscillation amplitude. Different kinds of attachments are proposed in the literature. Among the first, Den Hartog [12] proposed a linear vibration absorber, realized with mass, dashpot and spring and gave analytical expressions for the optimal tuning of the absorber frequency and damping factor, based on the equal peak method of the primary structure frequency response function. According to his formula, the optimal

frequency ratio between the main structure and the absorber, is found to be around the unity. Following the Den Hartog viscoelastic tuned mass damper (VTMD), other researchers proposed later many different alternatives of attachments and design approaches, fundamentally employing linear elements [13-16], introducing different optimization criteria [17, 18], even with attention to the specific loading conditions [19, 20].

In the literature a few proposal of nonlinear attachments can also be found, as those in [21-23], whereas in the last two decades there was an explosion of studies devoted to the introduction of solutions based on attachments with nonlinear restoring forces, after a series of papers [24-26] devoted to analyze the energy transfer in dynamics of systems connected with a small nonlinear oscillator. Similar dynamic phenomena are observed for systems with hysteresis, a nonlinearity which offers an intrinsic damping [27, 28].

So, many recent papers deal with nonlinear absorbers for vibration passive mitigation, different solutions are investigated, mostly adopting absorbers characterized by polynomial or other single-valued laws [29-37]. Other solutions involve absorbers characterized by hysteresis, where this choice depends on the material adopted, like rubber, SMA, cables, [38-46].

In this context, the idea of attaching a vibration absorber to the barrier columns is considered here as a possible solution for reducing vibrations. Recent studies [27, 28] show that a hysteretic absorber in different internal resonance conditions with the primary structure can effectively reduce the amplitude and number of vibration cycles of a main structure. Due to the strong nonlinearity, the absorber has stiffness and damping properties dependent on the displacement amplitude and for this reason it must be optimally tuned. The main aim of this study is thus modelling, design and experimental validation of a hysteretic vibration absorber (HVA) with optimized performances as an effective solution for mitigating the vibrations induced on noise barriers of railway high speed lines. The innovative strategy proposed mitigates the barrier vibrations by improving its low dissipative capabilities, taking advantage of the energy transfer in the relative motion between the barrier and the hysteretic absorber. The barrier is modelled as a generalized single degree of freedom system, whereas the absorber, which has light mass, is attached to the main structure with a connection element described by the Bouc-Wen hysteretic model. Advantageous conditions, for control purposes, are obtained when the two oscillators are close to a resonance condition (1:1). A parametric analysis varying the hysteretic absorber characteristics, obtained by a preliminary design, is carried out and the optimal values of the absorber parameters are obtained by maximizing a performance index of the barrier response to the train excitation. The absorber is realized using four high damping rubber elements, which have the advantage of directly representing the elastic and damping components in a single element. Its properties are characterized through experimental tests and an identification of the constitutive parameters is carried out. The validation of the realized absorber effectiveness is assessed by performing dynamic analysis on the two degrees of freedom (2DOF) system with the train excitation. Moreover, it is shown that the absorber optimization can be pursued by analyzing the free response, condition that can be experimentally investigated much more easily. Finally, since the optimal design of the nonlinear absorber is amplitude dependent, a sensitivity analysis of its performances varying the train velocity is also reported.

2. Noise Barriers and Excitation

Noise barriers for high speed lines are generally composed of H section steel profile columns, spaced every 3 m, constrained to the base through anchor bolts and noise panels inserted between the profile flanges, Fig. 1a. These panels are usually made of metal (aluminum, stainless steel or galvanized steel), concrete, or transparent material (glass or PMMA), as well as a combination of same, depending on environmental aspects and costs. Figure 1b shows the plan of a barrier made with concrete noise panels.

The distribution of the pressures along the barrier's height due to the passing train, $p(y)$ is not constant, reaching a maximum at the lower part, Fig. 2a. The variation with the vertical abscissa y has been experimentally obtained from in situ measurements and it is described by a polynomial function, depending on the train's speed and the rail-barrier distance [4]. By observing the behavior along the longitudinal direction, the pressure wave propagates with speed equal to that of the train. The pressure dynamic signal is characterized by two main not symmetrical impulses, corresponding to the head and tail of the train, connected by oscillations of minor amplitude, as reported in Fig. 2b where the normalized time history of the excitation $g(t)$ is depicted. The time interval of the pressure dynamic signal is a function of the train velocity. By examining the Fourier transform of the pressure dynamic signal in the frequency domain it can be observed that the main amplifications are in the range of 0-5 Hz, with a maximum around 2.7 Hz for a train speed of 325 kph.

Experimental outcomes, obtained during testing campaigns on noise barriers [4], evidenced the dynamic interaction with the train increasing with the velocity. Concerning the structural response of the noise barriers, the time-history develops through a higher number of cycles compared to those of the input pressure, which is important for the column fatigue phenomenon. Moreover, tests and finite element analyses conducted on the barriers showed that the columns substantially behave in the first mode and each one deflects independently from the others [4]. For this reason, it seems reasonable to model each column, with the associated part of paneling, independently as a generalized single degree of freedom (SDOF) system, Fig. 1c.

Columns of noise barriers are cantilever beams with distributed mass $m(y)$ and flexural rigidity $EI(y)$, functions of the abscissa y along the barrier height ($0 \le y \le H$). The deflection of the beam is described by a shape function $\psi(y)$, that approximates the fundamental vibration mode, multiplied by the displacement quantity $x_1(t)$. The equation of motion of the generalized SDOF system is:

$$m_1 \frac{d^2 x_1}{dt^2} + c_1 \frac{dx_1}{dt} + k_1 x_1 = F(t) \tag{1}$$

with generalized mass m_1, stiffness k_1 and force induced by train passage $F(t) = F_1 g(t)$ defined by:

$$m_1 = \int_0^H m(y)[\psi(y)]^2 dy, \qquad k_1 = \int_0^H EI(y)[\psi''(y)]^2 dy, \qquad F_1 = \int_0^H q(y)\psi(y)dy \tag{2}$$

where $q(y)$ is the distributed load for unity of column length, $q(y)=p(y)\cdot i$, with i interaxle spacing between two columns, Fig. 1b.

The natural circular frequency of the SDOF system is $\omega_1 = (k_1 / m_1)^2$, whereas the damping coefficient is given by $c_1 = 2\xi_1 m_1 \omega_1$, where ξ_1 is the structural damping factor. The presented case study refers to a 4 m high rail noise barrier, made with H section steel columns and concrete paneling. The structure is a cantilever beam with a 3 m wide paneling area, equal to the interaxle spacing between two columns. The total mass m_1 is estimated considering the sum of the column and the paneling masses and a damping factor $\xi_1 = 2\%$ is assumed according to the experimental results [11]. Table 1 summarizes the geometrical and inertial characteristics of the generalized SDOF system considered.
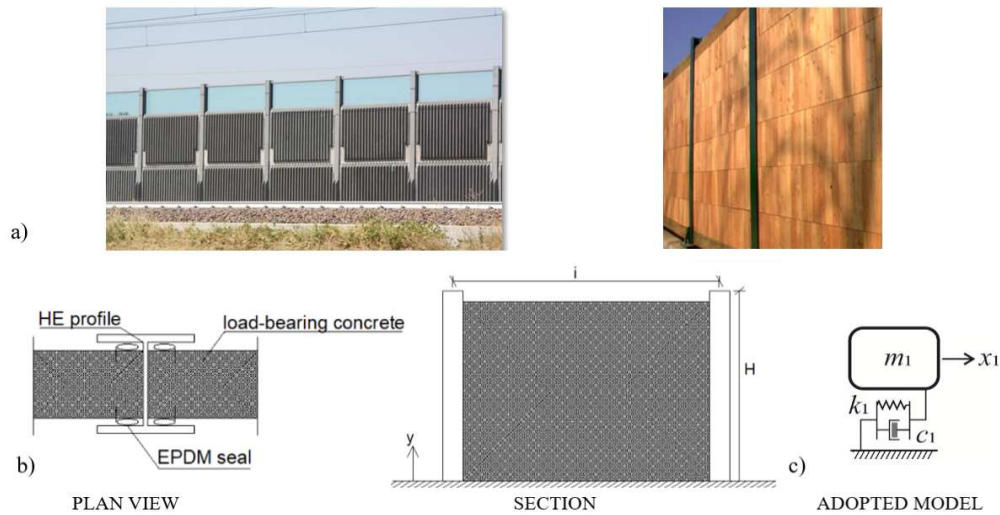
Fig. 1. a) Barriers types on HSLs, b) column and concrete barrier plan and vertical section, c) schematic representation of the model adopted for the barrier.
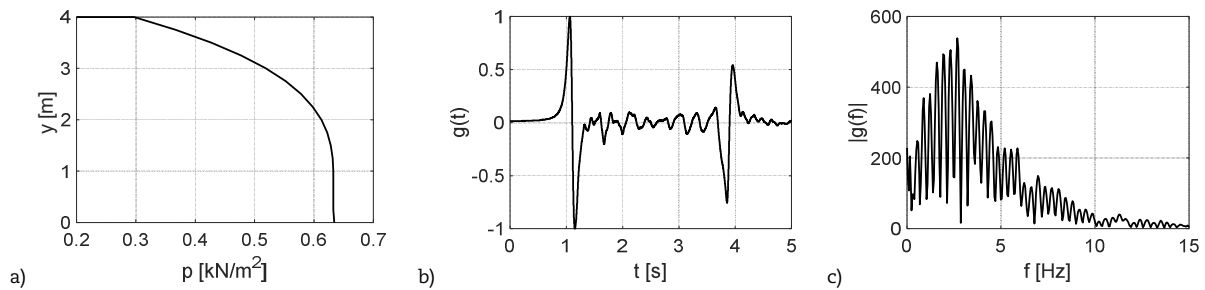

Fig. 2. a) Train forcing hydrodynamic pressure along the barrier's height and b) normalized forcing action time history, for train velocity 325 kph, c) Fourier transform of the forcing action.

It is worth noticing that the barrier frequency f_1=5.65 Hz is not in the zone of maximum amplification of the train forcing action, which has a maximum peak around 2.7 Hz for a train velocity of v=325 kph, nevertheless, its safety against fatigue is not satisfactory, since the structure is subjected to numerous high stress cycles. As shown in the following Sections, the primary structure with the attachment is modelled as a 2DOF oscillator, Fig. 3a.

3. Hysteretic Attachment Constitutive Model

The restoring force $f(x)$ of the attachment has a hysteretic behavior described by the Bouc-Wen model [47, 48]:

$$f(x) = k_2 x + z(x) \qquad (3)$$

where $x=x_2-x_1$ is the relative displacement between the two masses m_1 and m_2, Fig. 3a. The hysteretic part $z(x)$ is obtained by the following nonlinear differential equation:

$$\frac{dz}{dt} = \left\{ k_d - \left[\gamma + \beta \, \text{sgn}\left(z \frac{dx}{dt} \right) \right] | z |^n \right\} \frac{dx}{dt} \qquad (4)$$

where the quantities k_d, γ, β, n are the constitutive parameters of the Bouc-Wen law. The positive exponential parameter n is taken equal to 1; this value of n is suitable in the simulation of many applications and ensures that the transition from elastic to the post-elastic branch is not abrupt.

The hysteretic loops of the restoring force (Fig. 3b) can be obtained in closed form as described in [28], where it has been shown that the behavior of the hysteresis loop can be significantly modified by varying the parameters β and γ: the case $\gamma / \beta = 1$ corresponds to a fully hysteretic loop which exhibits the maximum energy dissipation, the case $\gamma / \beta > 1$, which is represented by the red curve in Fig. 3b, leads to a reduction of the energy dissipation. Only the case $\gamma / \beta = 1$, which is more suitable to the application herein dealt with, is considered. It is worth noticing that, as shown in Figs. 3c and 3d, the stiffness and damping characteristics of the hysteretic absorber depend on the cycle amplitude $\overline{x}$. In particular, the equivalent stiffness k_e as a function of $\overline{x}$ can be expressed in the following form [28]:

$$k_e(\overline{x}) = k_2 + \frac{k_d}{\overline{x}(\beta + \gamma)} \left(1 - e^{-\overline{x}(\beta + \gamma)} \right) \qquad (5)$$

Table 1. Dynamic properties of the primary system.

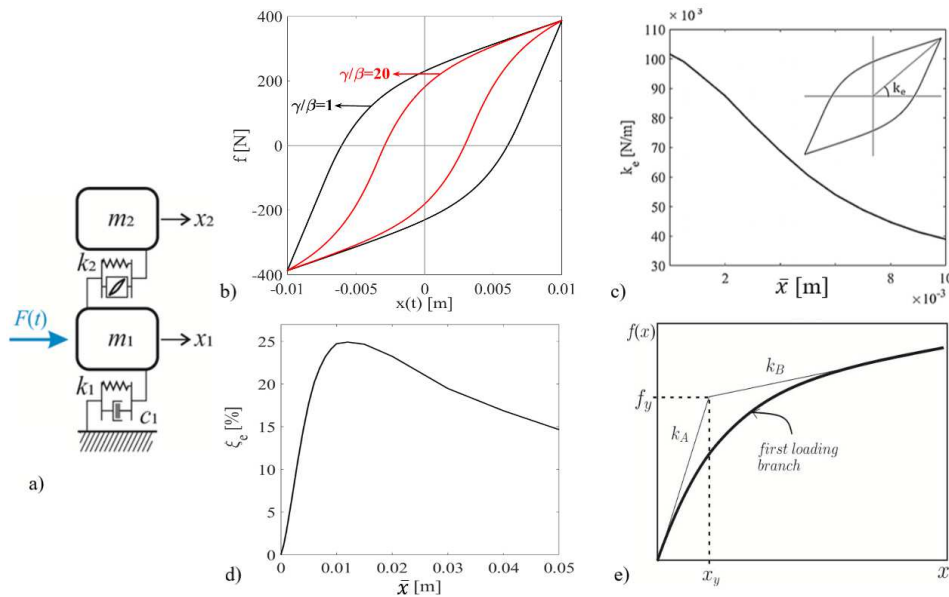| m_1 [kg]	k_1 [N/m]	c_1 [N sec/m]	F_1 [N]	f_1 [Hz]
1220.7	1.5326 10^6	1730.1	1840.1	5.65

Fig. 3. System under investigation. a) 2DOF mechanical model; b) Bouc-Wen restoring force loops for $\gamma/\beta = 1$ and 20; c), d) the secant stiffness k_e and damping factor ξ_e versus the cycle amplitude $\bar{x}$; e) first loading branch.

Furthermore, the equivalent damping ratio ξ_e, defined as the value of damping of a viscoelastic device which dissipates the same energy of the HVA in a cycle of amplitude $\bar{x}$, is given by:

$$\xi_e(\bar{x}) = \frac{1}{2\pi k_e \bar{x}^2} \oint z(x)dx \tag{6}$$

According to Eq. (6), the damping factor reaches a maximum at some displacement amplitude, then decreases, Fig. 3d.

As far as the stiffness properties of the device are concerned, it should be observed that, according to Eq. (5), the equivalent stiffness decreases with the amplitude varying from $(k_2 + k_d)$ to k_2:

$$\lim_{\bar{x} \to 0} k_e(\bar{x}) = k_2 + k_d, \qquad \lim_{\bar{x} \to \infty} k_e(\bar{x}) = k_2 \tag{7}$$

Thus, the hysteretic absorber possesses an initial stiffness $(k_2 + k_d)$ denoted hereafter with k_A, and a post-elastic stiffness k_2 denoted with k_B; their ratio is the hardening coefficient $\delta (\delta < 1)$:

$$k_A = k_2 + k_d, \qquad k_B = k_2, \qquad \delta = \frac{k_B}{k_A} \tag{8}$$

Finally, Fig. 3e shows the first loading branch and the bilinear curve characterized by the initial and post-elastic stiffness k_A and k_B: the intersection point of the bilinear curve identifies the force f_y and the displacement x_y at yielding.

4. Equations of Motion of the Structure with Attachment

According to the previous sections, the noise barrier with the attachment of mass m_2 is modelled as 2DOF oscillator, Fig. 3a. The dimensional equations of motion of system subjected to a time-dependent force $F(t)$ can be written in the following form:

$$m_1 \frac{d^2 x_1}{dt^2} + c_1 \frac{dx_1}{dt} + k_1 x_1 - k_2 x - z(x) = F(t) \tag{9}$$

$$m_2 \frac{d^2 x_2}{dt^2} + k_2 x + z(x) = 0 \tag{10}$$

$$\frac{dz}{dt} = \left\{ k_d - \left[\gamma + \beta \, \text{sgn}\left(z \frac{dx}{dt} \right) \right] | z |^n \right\} \frac{dx}{dt} \tag{11}$$

where, as already introduced, $x = x_2 - x_1$. As it has been shown in Section 3, the hysteretic attachment has a stiffness depending in a nonlinear way on the relative displacement amplitude and varying from k_A for small amplitudes to k_B for large displacements, Eqs. (7)-(8). As a consequence, the nonlinear frequencies of the system depend on the amplitude as well and vary from ω_{iA} to ω_{iB} according to the following equations [28]:

$$\omega_{1A,2A}^2 = \frac{(\nu + \mu\nu + \mu\delta) \mp \sqrt{(\nu + \mu\nu + \mu\delta)^2 - 4\mu\nu\delta}}{2\delta\mu} \omega_1^2 \tag{12}$$

$$\omega_{1B,2B}^2 = \frac{(\mu + \nu + \mu\nu) \mp \sqrt{(\mu + \nu + \mu\nu)^2 - 4\mu\nu}}{2\mu} \omega_1^2 \tag{13}$$
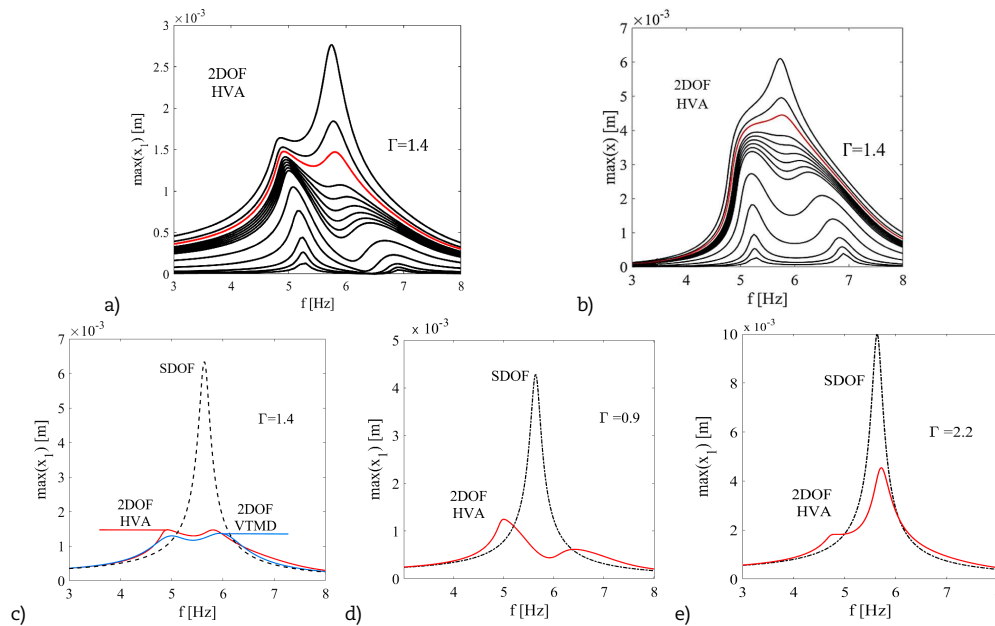
Fig. 4. 2DOF near (1:1) internal resonance. Frequency-response curves of x_1 (a) and x b) for increasing amplitude (Γ=0.5-2.5); c)-e) comparison with the SDOF system response for different forcing amplitudes. Optimal case (c) and detuning (d and e).

where $\mu = m_2/m_1$ and $\upsilon = k_2/k_1$ denote the ratio between masses and elastic stiffness of the primary structure and the attachment.

5. Internal Resonance (1:1)

Linear viscoelastic attachments have been extensively studied in the literature [12-20] and the criterion proposed by Den Hartog [12] for an optimal vibration mitigation has been exploited in many numerical studies. However, in real cases, e.g. when rubber elements or steel wire ropes are adopted to build the device, it has been observed that the viscoelastic behavior cannot satisfactorily describe the restoring force of the attachment [46]: hysteretic models are more suitable to represent the actual behavior.

Thus, in the present study, it is considered a hysteretic absorber designed near the (1:1) internal resonance condition, by analogy with the linear viscoelastic case proposed by Den Hartog, where the frequency of the attachment is close to the frequency of the primary system. To this end, suitable initial parameters of the system are adopted: a mass ratio μ=m_2/m_1=0.05 with respect to the primary structure mass, which guarantees a light absorber and a ratio between stiffnesses υ=k_2/k_1=1/105. They lead to an initial frequency ratio r_A=ω_{2A} /ω_{1A} close to 1.35, which is candidate to reach the optimal value with increasing oscillation amplitude. A fully hysteretic loop is adopted for the Bouc-Wen law with β=γ=180 and δ=0.15.

The main dynamic characteristics of the 2DOF system are well described by the frequency response curves of the primary structure subjected to a sinusoidal force, $F(t) = \Gamma f_y \sin(\Omega t)$. Unlike the linear tuned mass damper, the behavior of the hysteretic attachment and its effectiveness depend on the excitation level Γ. In particular, Figures 4a and 4b report, for increasing excitation amplitudes, the frequency response curves of the primary structure displacement and of the absorber relative displacement. Figures 4c and 4e illustrate the comparison of the structure response with (solid line) and without (dotted line, primary SDOF system) hysteretic attachment for three excitation amplitudes. For low values, Fig. 4a and 4b, the ratio between the two resonance frequencies is greater than the optimal value, around 1.2; the equivalent stiffness is greater than the optimal k_0 and the first resonance peak is higher than the second one, due to the detuning circumstance, as also shown in Fig. 4d. For increasing amplitude, in the excitation range near Γ=1.4 (red curve in Fig. 4a,b), the stiffness and damping of the hysteretic attachment reach their optimal values corresponding to a frequency response exhibiting two equal peaks; for this intensity the effectiveness resembles that of a viscoelastic tuned mass damper (VTMD) with a remarkable mitigation of the primary system vibrations. This is clearly shown in Fig. 4c, where, around ω_1 the maximum response amplitude of the primary system experiences about a 80% decrease when the hysteretic attachment is present (red line); in the same figure the ideal case of the VTMD is shown by the blue curve. For larger excitations, Fig. 4e, the equivalent stiffness is lower than the optimal k_0 and the peak of the second mode is amplified: then the mitigation capability of the hysteretic attachment is weakened with a reduction of about 35%. It can be stated that an optimal excitation range for the functioning of the hysteretic attachment is around Γ=1.4.

This investigation is very useful in the initial design procedure because it provides the range of oscillation amplitudes (red curve in Fig. 4b) where the absorber is effective. This range of amplitudes should be experienced by the primary system and the absorber under the non-stationary train loading.

6. Parametric Analysis and Design of the Hysteretic Vibration Absorber

The design of the hysteretic absorber to reduce the vibrations of the barrier (whose dynamic properties are reported in Table 1) due to the train passage implies a proper choice of the parameters m_2, k_2, k_d, β, γ, n. According to the results synthetically described in Fig. 4, for the steady-state vibrations the absorber parameters must be selected in such a way to reach the stiffness k_0 at the oscillation amplitude of the optimal linear tuned mass damper under the same external force. Since the structure response under the train is nonstationary, the optimal values of the parameters are determined by updating the initial values through a parametric analysis.

The absorber mass is chosen, as in Section 5, in order to have a mass ratio μ=m_2/m_1=0.05. The stiffness k_2 and k_d are calibrated by varying the initial stiffness k_A and the hardening ratio δ, Eq. (8). The initial stiffness has been assumed greater than the optimal stiffness of a viscoelastic absorber, k_0=67768 N/m, designed for the same action according to Den Hartog theory [12], as

$k_A = \alpha k_0$ with $\alpha > 1$, and it is varied by changing α among the values 1.5, 1.7, 1.9. For the hardening ratio δ two values have been assumed: 0.15 and 0.30. Concerning the parameters governing the hysteresis shape, full hysteresis laws are adopted with $\beta = \gamma$ and varying them in the range 10-450, whereas n has been assumed equal to 1.

To assess the effectiveness of the absorber to mitigate the vibration of the barrier, a performance index evaluated on the basis of the rms of the response is considered:

$$i_p = \left(1 - \frac{rms(x_{1HVA}(t))}{rms(x_{1NA}(t))}\right) \tag{14}$$

where $x_{1HVA}(t)$ and $x_{1NA}(t)$ are the primary system displacements with the HVA attachment and with no attachment (NA), respectively. By maximizing the index i_p, the design parameters of the absorber are obtained. Since the tuning of the absorber depends on the loading intensity, it is considered a pressure corresponding to a train at reference speed of 325 kph.

The response of the system to the train pressure is obtained by numerically integrating the equations of motion (9)-(11). The performance index for the two values of the hardening ratio δ and three values of the initial stiffness is reported versus β in Fig. 5a. For each curve with given initial stiffness and hardening ratio, there exists a β value that maximizes the performance index indicated with vertical lines. By increasing the initial stiffness and the hardening ratio, once reached the maximum, the slope of each curve becomes less steep. Optimal β^* increases by increasing the initial stiffness, it is modestly influenced by the hardening ratio for high values of the initial stiffness, but, at the lowest value of initial stiffness, the maximum performance index of 0.42 is reached at the same optimal β^*=180, obtained for both values for δ=0.15 and 0.30. It is worth noticing that, for the same amplitude, the restoring force reaches higher values by increasing the hardening ratio, moreover the most dissipative cycles, for given δ, are obtained for the lowest value of the initial stiffness. Although the shape of the two cycles for lowest initial stiffness is quite different, the response in terms of performance index is substantially analogous (i_p =0.42).

It seems interesting to analyze the performance of the same system with respect to free vibrations. In fact, the impulsive action has similarities with the forcing action of the train, but this case can be more simply reproduced with experimental tests. The initial conditions, given in terms of displacement of the two masses, correspond to the maximum displacement of the barrier with no attachment for train passage at speed 325 kph: $x_1(0)=x_2(0)$ =3.4 mm.
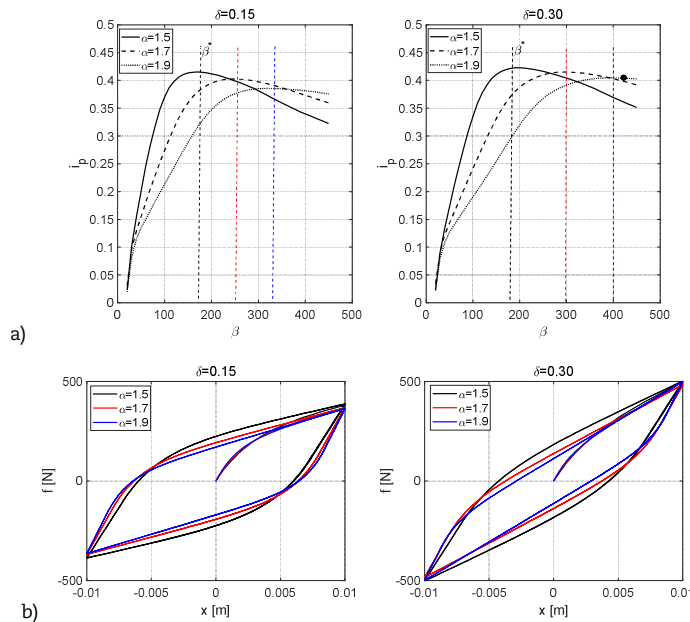

Fig. 5. Parametric analysis with train excitation at v=325 kph. a) The performance index versus β for three values of α, and δ = 0.15, 0.30. The vertical lines indicate the optimal β for each curve (the black dot represents the i_p value for the parameters experimentally identified in Sect. 8); b) force displacement hysteretic cycles in the optimal cases for δ =0.15 and δ=0.30.
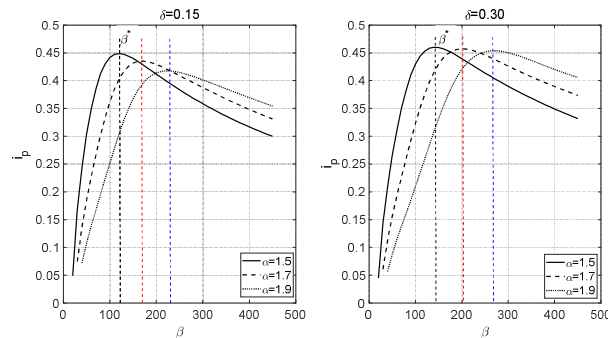

Fig. 6. Free vibrations with initial displacement $x_1(0)=x_2(0)$ =3.4 mm. The performance index versus β for three values of the parameter α and δ = 0.15, 0.30. The vertical lines indicate the optimal β for each curve.

Table 2. Design parameters of the hysteretic absorber.

k_2 [N/m]	k_d [N/m]	$\beta=\gamma$ [1/m]	n	δ
30480	71121	180	1	0.30

In Fig. 6, the parameter sensitivity analysis, previously performed for the train excitation, is repeated for the case of free oscillations. It can be noticed that, also in this case, each curve with given initial stiffness and hardening ratio exhibits a maximum performance index at a specific β value. All curves have a well-defined maximum and then decrease: optimal β^* increases with the initial stiffness and the hardening ratio. However, when the initial stiffness is low, optimal β^* is similar for the two hardening ratios considered and is similar to that obtained with the train forcing action. The choice that maximizes the performance index is the one with $\alpha=1.5$ and $\delta=0.30$, as in the case of the train, and maximum i_p of 0.46 is obtained for $\beta=\beta^*=150$. The results of the optimization procedure are very close to those considering the train loading.

The design parameters of the hysteretic absorber, selected from the parametric analysis, under the train excitation, are reported in Table 2.

7. System Response

The response of the 2DOF system, which represents the barrier with the hysteretic absorber designed as discussed in Section 6, to train excitation and to initial conditions (free vibrations) is reported in terms of displacement time history of the barrier and force displacement hysteretic cycles of the absorber. For comparison purposes, the responses obtained in the case of the ideal viscoelastic absorber are also reported.

7.1 Train excitation

The response of the barrier with hysteretic absorber (HVA) and with no attachment (NA) to the train passage is shown in Fig. 7a. The time history has two peaks corresponding to the head and tail of the train, with first peak greater than the second and lower amplitude cycles in between. By comparing the two responses, the effectiveness of the hysteretic vibration absorber emerges: after first few oscillations in fact, the response is efficiently reduced. The number and amplitude of the oscillation cycles between the two pulses and after the second one is reduced and this is crucial to prevent the fatigue phenomenon typical of these structural elements. Figure 7b shows the hysteretic cycle of the absorber which has maximum displacement around 6.6 mm and restoring force around 400 N, corresponding to the main pulse and then the absorber experiences cycles of lower amplitude. The performance index reached is i_p=0.42. For comparison, in Fig. 7c the response of the barrier with a VTMD is reported; only slight differences can be observed in the time-history of the primary system, exhibiting a performance index i_p=0.43. In Fig. 7d the cycles of the restoring force, sum of damping and elastic components, is reported for completeness.

7.2 Free vibrations

Figure 8a shows the barrier response to free vibrations and non-zero initial displacement with hysteretic absorber (HVA) and no attachment (NA). The displacement time history when adopting the hysteretic absorber is immediately reduced after the first oscillations and tends to zero after few seconds. The effectiveness of the control system is evident comparing the response with no attachment. Figure 8b shows the hysteretic cycle of the absorber which has a maximum displacement around 8 mm and restoring force lower than 500 N, few cycles of higher amplitude are then followed by cycles of modest amplitude. The performance index reached in this case is i_p=0.46. For comparison, in Fig. 8c,d the time history response and restoring force loops, when a VTMD is used, are reported; also in this case, slight differences can be observed in the time-history of the primary system, exhibiting the same performance index i_p=0.46. These results show that the analysis of free oscillations is able to give similar results obtained using the actual train excitation. This is only of a little importance in the numerical investigations, but it is of great importance when an experimental validation of the absorber effectiveness is pursued.

8. Prototype Absorber and System Response

8.1 Experimental characterization of the absorber

Based on the design presented in Section 6, the hysteretic absorber has been made of a mass realized with a square steel plate of 61 kg placed on four high damping rubber elements in proximity to the plate corners. Each element has 20 mm diameter with a total of 8 mm rubber thickness and 1 mm of steel shim in order to achieve the target shear strain around γ_s=100%, corresponding to the expected maximum displacement of the HVA. The nominal equivalent horizontal stiffness of each rubber element is 16000 N/m and the shear modulus of the blend is 0.4 MPa. A sketch of the element is reported in Fig. 9a showing plane and lateral view.

Characterization tests have been conducted on each rubber element at different values of the shear strain γ_s=25, 50, 100%. Cyclic tests at prescribed displacement were performed using the Zwick-Roell universal testing machine at a frequency of 0.2 Hz, Fig. 9a. The machine load cell and displacement transducer were utilized to measure force and displacement. For each test, five cycles have been made and the constitutive parameters are estimated on the third cycle; the experimental results are reported in Fig. 9b.

An identification procedure has been applied to determine the optimal constitutive parameters by minimizing the difference between experimental and analytical values of the restoring force, which are furnished by the Bouc-Wen model, Eqs. (3)-(4), and depend on the parameters vector $\underline{c}=\{k_2,k_d,\beta\}^T$, having assumed $n=1$ and $\beta=\gamma$. An initial guess vector $\underline{c}_0=\{k_{20},k_{d0},\beta_0\}^T$ is chosen in an appropriate range of values. Due to measurement noise and model error, the constitutive parameters are determined by minimizing the function $b(\underline{c})$:

$$b(\underline{c}) = \frac{1}{N}\sum_{i=1}^{N}\left(\frac{f_i(\overline{c})-\tilde{f}_i}{\tilde{f}_a}\right)^2 \tag{15}$$

where N is the number of time instants t_i at which the experimental and analytical force, $\tilde{f}_i$ and $f_i(\overline{c})$ respectively, are compared, and $\tilde{f}_a$ is a mean value of the experimental force used to normalize the difference.

The numerical restoring force is computed at each displacement d_{i+1} as:

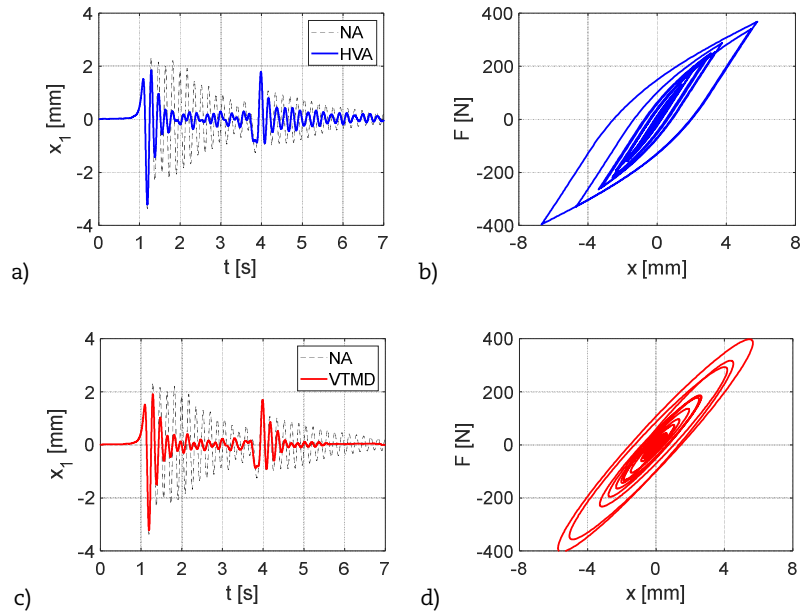$$f_{i+1} = k_2 d_{i+1} + z_{i+1} \tag{16}$$

Fig. 7. a) Time history of the primary structure displacement with no attachment (NA) and with HVA; b) restoring force hysteretic loop; c), d) VTMD attachment: time history of the primary structure and restoring force loop. Train speed 325 kph.
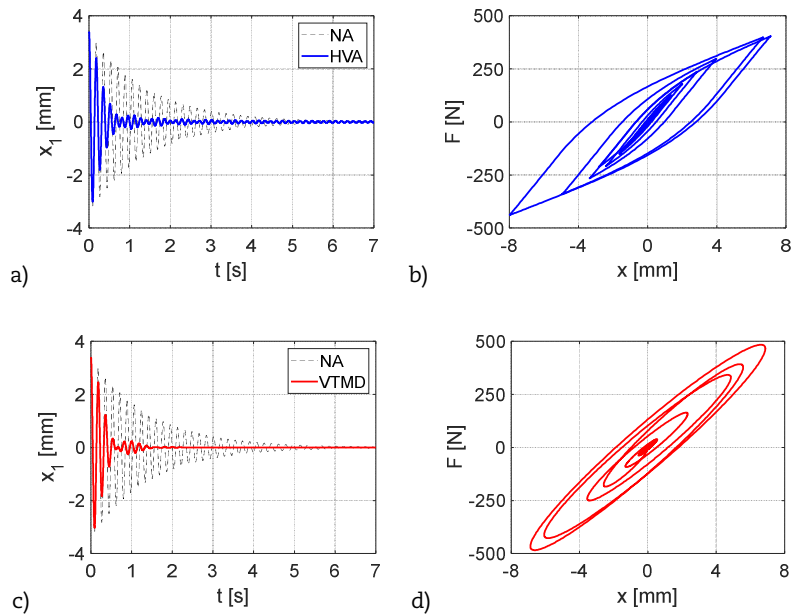

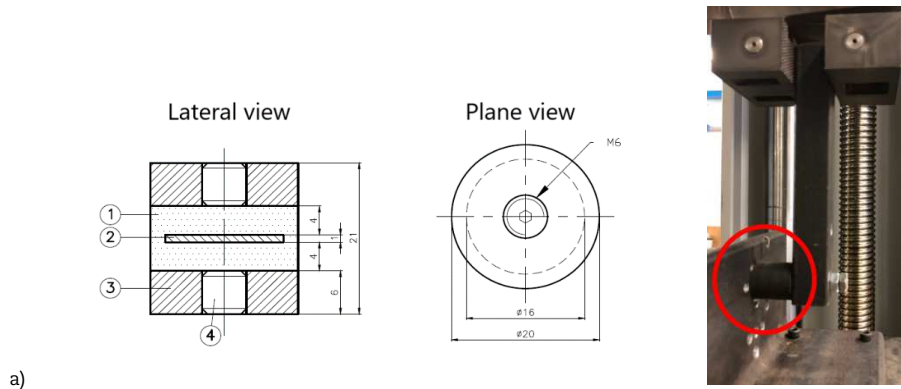**Fig. 8**. a) Time history of the primary structure displacement with no attachment (NA) and with HVA; b) restoring force hysteretic loop; c), d) VTMD attachment: time history of the primary structure and restoring force loop. Free vibrations $x_1(0)=x_2(0)=3.4$ mm.

Fig. 9. a) Sketch of the hysteretic absorber and experimental setup, Legend: 1) rubber layer, 2) steel shim, 3) connection plate, 4) hexagonal hollow screw; b) experimental loops at different values of the shear strain γ_s; c) comparison of the numerical and experimental hysteresis loops for different values of the shear strain γ_s.
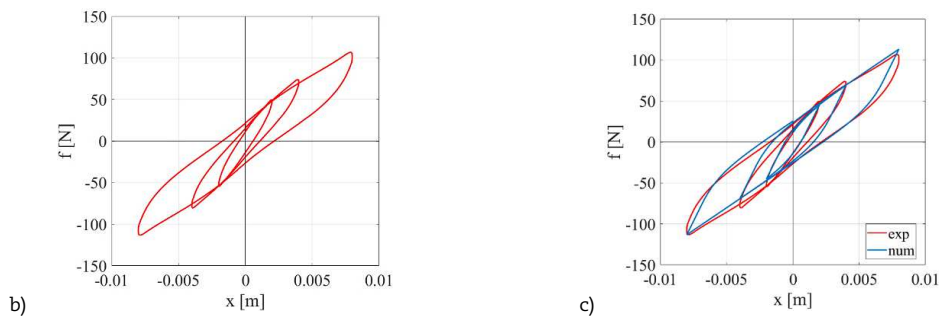
b)

c)

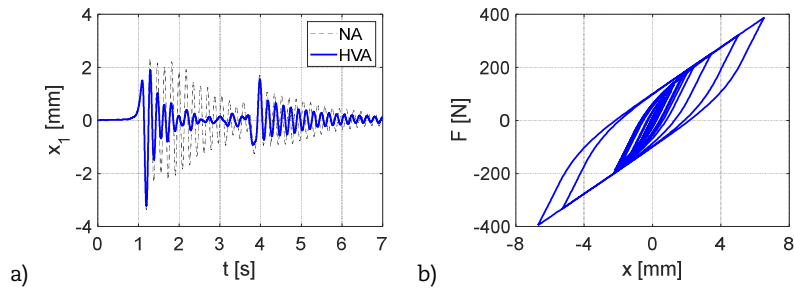**Fig. 9.** Continued.

a)

b)

Fig. 10. a) Time history of the primary structure displacement with no attachment (NA), and HVA experimentally identified; b) Force displacement loops. Train speed 325 kph.

and

$$\frac{z_{i+1} - z_i}{d_{i+1} - d_i} = k_d - \left[\gamma + \beta \, \mathrm{sgn}\left(v_i z_i\right)\right] |z_i|^n \tag{17}$$

evaluated by central difference method with $v_i = (d_{i+1} - d_i)/\Delta t$.

At the end of the process, the suitability of the set of parameters identified is estimated computing the mean error between experimental and numerical data evaluated with the identified parameters:

$$e = \frac{1}{N} \sum_{i=1}^{N} \frac{|f_i(\bar{c}) - \tilde{f}_i|}{\tilde{f}_a} \tag{18}$$

Cyclic tests at the three different shear strain values have been utilized in the identification with the aim to find an optimal set capable to describe accurately the experimental response at different amplitudes. In Fig. 9c, the results of the identification are shown in terms of hysteretic cycles, comparing the experimental and numerical response at the three amplitudes. The identified model (Table 3) fits satisfactorily well the experimental response. The identified initial stiffness, k_A, corresponds to coefficients α=1.9 and δ=0.3 which is close to one of the constitutive loops reported in Fig. 5b, case α=1.9, δ=0.3, β=400.

The realized absorber, with parameters experimentally identified (α=1.9 and δ=0.3, β=430) and slightly different from the optimal values, still has advantageous performances i_p =0.41 near to the optimal case, as represented with a black dot in Fig. 5a, due to the flatness around the maximum of the curve.

8.2 System response

The response of the 2DOF system with the actual absorber, whose parameters were experimentally identified (Table 3), to train excitation and free vibrations is shown in terms of displacement time history of the barrier and force displacement hysteretic cycles of the absorber in Figs. 10 and 11 respectively.

In Fig. 10 the effectiveness of the realized absorber is evident by comparing the two responses with (HVA) and without attachment (NA). The reduced number and amplitude of the oscillation cycles well contrast the barrier fatigue. Figure 10b shows the hysteretic cycle of the absorber which has maximum displacement around 6.7 mm and restoring force lower than 400 N, at the main pulse. The cycle shape, which differs from the target one reported in Fig. 7b, still guarantees high dissipative capacities and the performance index is i_p =0.41 similar to the value of the optimized absorber, as said before.

Figure 11a shows the response of the barrier to non-zero initial displacement with (HVA) and without attachment (NA). Also in this case, the response of the primary structure with hysteretic absorber is immediately reduced and rapidly goes to zero. Figure 11b shows the cycles of the absorber which has maximum displacement around 8.4 mm and restoring force lower than 500 N; few cycles of higher amplitude are followed by cycles of low amplitude. Even in this case, free oscillations give similar results of the forced response about the absorber effectiveness.

Table 3. Identified parameters of one of the four elements that realize the hysteretic absorber having assumed n=1 and β=γ

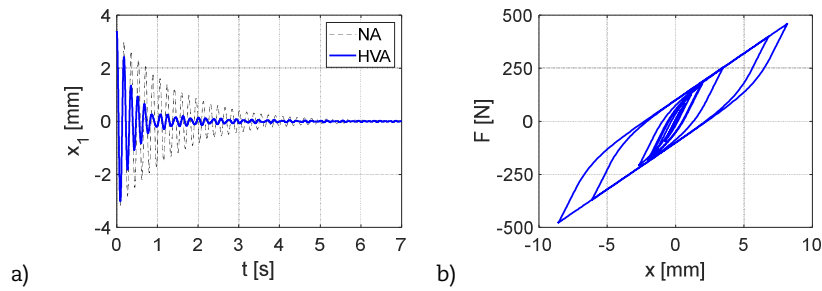| k_2 [N/m]	k_d [N/m]	β [1/m]
10960	21750	430

Fig. 11. a) Time history of the primary structure displacement with no attachment (NA) and HVA experimentally identified; b) Force displacement hysteretic loops. Free vibrations $x_1(0)=x_2(0)=3.4$ mm.
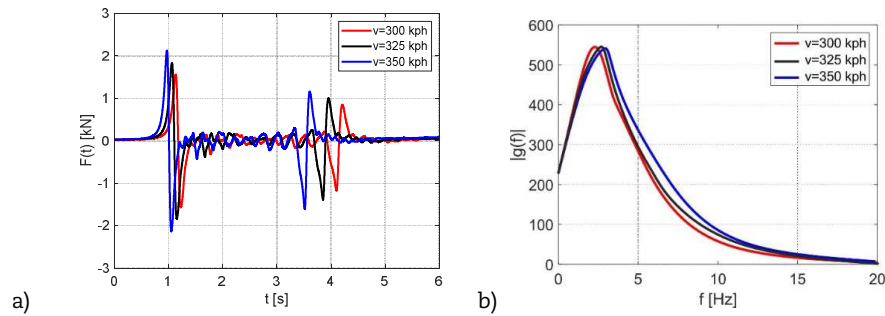

Fig. 12. a) Forcing action time history for three different train speeds; b) Fourier transform envelope.
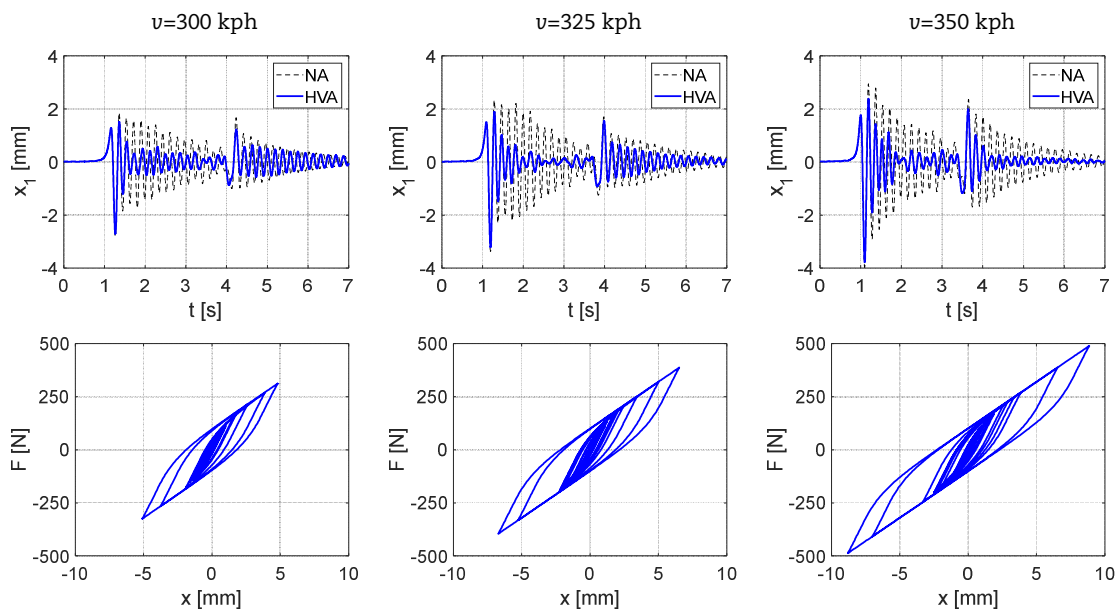

Fig. 13. Time histories of the primary structure displacement with no attachment (NA), and HVA experimentally identified. Force displacement hysteretic loops of the HVA. Train speed $v=300, 325, 350$ kph.

9. Sensitivity analysis to train speed variations

The design and tuning of the hysteretic absorber were made with reference to a train speed of 325 kph. It was shown however, that the absorber performance depends on the oscillation amplitude, which is related to the excitation intensity. It is therefore useful to assess its performance with a sensitivity analysis varying the train speed in order to verify the consequence of a possible detuning. In the analysis a decreased value of 300 kph and an increased value of 350 kph with respect to the reference case are investigated. These boundary values were chosen considering that train speeds lower than 250 kph do not produce appreciable dynamic amplification of the barriers response, whereas the upper value of 350 kph is a limit for the high speed line and train design.

Figure 12 depicts the time history of the forcing action and the Fourier transform envelope of the signals for the three speed values. By observing the input time history in Fig. 12a, it is possible to notice that increasing the speed the amplitudes of the two main pulses increase while the time interval of the action decreases. It reflects on the frequency content, Fig.12b, which has the main amplification that moves to higher frequencies when the speed increases while the amplitude and shape of the envelope do not change noticeably. It is evident that at lower speeds the frequency content of the action moves away from the resonance of the barrier and the dynamic amplification is therefore reduced, instead by increasing the speed the main action frequency content moves closer to the barrier frequency and for this reason its effectiveness must be verified.

Table 4. Performance index values i_p varying the train speed.

	v = 300 [kph]	v = 325 [kph]	v = 350 [kph]
i_p designed HVA	0.36	0.42	0.39
i_p realized HVA	0.36	0.41	0.38

The performance indices estimated at the three different speeds for the 2DOF system equipped with the designed and the realized absorbers are reported in Table 4. For a decrease of the speed from the reference case, the performance index decreases, equally for the designed and realized absorbers, still reaching a quite high value. The frequency content of the action in this case is moving far from the resonance of the barrier; for this reason, the amplification is lower and the effectiveness of the absorber, which undergoes smaller relative displacements, diminishes. When the train speed is increased, also in this case the performance decreases, however still guaranteeing good vibration reductions, indeed the index i_p ranges between 0.39-0.38 for the designed and realized devices. So, it can be noticed that also varying the trains speed the performances of both the designed and realized absorbers are very similar and effective as well.

Figure 13 reports the time history of the barrier displacement with hysteretic absorber (HVA) and no attachment (NA) and the relevant restoring force loops for the three velocities. It is possible to observe that as the speed increases the maximum displacement increases as well. The effectiveness of the hysteretic absorber slightly decreases when the speed is different from that considered in the design (325 kph). In any case, for small variations of the train speed the absorber performance in reducing the barrier oscillations is still confirmed.

10. Conclusion

A strategy to mitigate the noise barrier vibrations due to the train passage in high speed lines was proposed in this paper. A nonlinear hysteretic vibration absorber, modeled, designed and experimentally identified, was attached to the barrier columns and, taking advantage of the relative motion between the two masses, the input energy was efficiently dissipated with a notable reduction of the primary structure response.

The barrier was modelled as a generalized single degree of freedom system, whereas the absorber was modelled with a light mass attached to the main structure through a hysteretic element described by the Bouc-Wen model. The equations of motion of the resulting 2DOF system were derived and for control purposes suitable conditions occur when the two oscillators, the primary structure and the attachment, are close to the resonance conditions (1:1). However, due to its hysteretic nature, the absorber behaves in nonlinear way and its stiffness and damping properties depend on the oscillation amplitude, reason why it must be carefully tuned.

The study of the response to harmonic excitation with increasing intensity is useful to understand that the absorber is effective in a well-defined range of oscillation amplitude, where an optimal tuning with the primary structure occurs and the equivalent stiffness and damping of the absorber resemble those of the optimal viscoelastic tuned mass damper. Since the response to train loading is nonstationary and the amplitude of oscillations is not constant, the characteristics of the hysteretic element assumed on the basis of the preliminary study under harmonic excitation are optimized by a parametric analysis varying its characteristics in a selected range and maximizing a performance index evaluated using the rms of the barrier response to the train excitation. Moreover, it has been shown that the optimal choice of absorber parameters can be suitably performed on the basis of the free vibrations. In fact, the same optimal constitutive law is obtained from free response; this result is of valuable interest because it is much easier to be experimentally reproduced and notably simplifies the experimental validations of the devices.

The hysteretic element of the absorber was realized exploiting the use of four high damping rubber elements and its constitutive parameters were identified through experimental laboratory tests. The effectiveness of the rubber absorber was assessed by performing dynamic analysis of the two degrees of freedom system under the train excitation and comparing its performances with those of the originally designed. It was shown that the realized absorber substantially behaves as the designed one in terms of performance index and barrier response reduction. Finally, a sensitivity analysis of the performance varying the train speed was reported. It was highlighted that even if the nonlinear absorber is amplitude dependent and requires a specific tuning, its effectiveness in the mitigation of the barrier response is confirmed in the most critical range of possible speeds for trains in the high speed railways.

Author Contributions

M. Basili planned the scheme, initiated the project and suggested the experiments; P. Casini developed the mathematical modeling and examined the theory validation; L. Morelli conducted the experiments and analyzed the empirical results; F. Vestroni supervised and checked the whole research. The manuscript was written through the contribution of all authors. All authors discussed the results, reviewed and approved the final version of the manuscript.

Conflict of Interest

The authors declared no potential conflicts of interest with respect to the research, authorship and publication of this article.

Funding

Nomenclature

b	Function to minimize for the identification	$p(y)$	Pressures distribution due to passing train
c_1	Generalized barrier damping coefficient	$q(y)$	Distributed load for unity of column length
$\underline{c}$	Vector of parameters to identify	r_A	Frequencies ratio at hysteretic initial stiffness
e	Error function	v	Train velocity
$EI(y)$	Distributed stiffness	$x(t)$	TMD relative displacement

$f(x)$	Attachment restoring force	$\bar{x}$	Hysteretic cycle amplitude
f_1	Barrier frequency	x_{1HVA}	Barrier displacement with hysteretic absorber
$\tilde{f}_a$	Mean value of the experimental force	x_{1NA}	Barrier displacement with no absorber
$\tilde{f}_i, f_i$	Experimental and analytical force	$x_i(t)$	Generalized displacement of barrier and TMD (i=1,2)
f_y	Yielding force	x_y	Yielding displacement
$F(t)$	Loading time history	y	Vertical abscissa
$g(t)$	Normalized loading time history	$z(x)$	Hysteretic part of the restoring force
H	Barrier height	β	Parameter regulating the shape of the hysteresis loop
i	Interaxle spacing between two columns	β'	Optimal value of the parameter
i_p	Performance index	γ	Parameter regulating the shape of the hysteresis loop
k_1	Generalized barrier stiffness	γ_s	Shear strain
k_2	Absorber post elastic stiffness	δ	Hardening coefficient
k_A	Absorber initial stiffness	μ	Mass ratio
k_B	Absorber final stiffness	υ	Stiffness ratio
k_d	Stiffness of the hysteretic component of the force	ξ_1	Barrier damping factor
k_e	Equivalent stiffness	ξ_e	Equivalent damping factor
k_0	Optimal stiffness	$\psi(y)$	Shape function
l_1	Generalized force due to train passage	ω_1	Barrier natural circular frequency
m_1	Generalized barrier mass	ω_{iA}	2DOF frequencies at hysteretic initial stiffness (i=1,2)
$m(y)$	Distributed mass	ω_{iB}	2DOF frequencies at hysteretic final stiffness (i=1,2)
n	Parameter regulating the transition of the hysteresis loop		

References

[1] Garai, M., Recent advances in noise barriers testing, qualifying and standardisation, *Proceedings of the Institute of Acoustics*, 32(3), 2010, 132-139.

[2] Su, W.Q., The Summary of Design of Railway Sound Barrier, *Journal of Railway Engineering Society*, 35, (8), 2018, 86-91.

[3] Xiong, X-H., Li, A.H., Liang, X.F., Zhang, J., Field study on high-speed train induced fluctuating pressure on a bridge noise barrier, *Journal of Wind Engineering & Industrial Aerodynamics*, 177, 2018, 157-166.

[4] Evangelista, L., Vittozzi, A., Silvestri, G., Theoretical and experimental evaluation of the noise barriers behavior on high speed lines, *Ingegneria Ferroviaria*, 64(1), 2009, 35-51 (in Italian).

[5] Tokunaga, M., Sogabe, M., Santo, T., Ono, K., Dynamic response evaluation of tall noise barrier on high speed railway structures, *Journal of Sound and Vibration*, 366, 2016, 293-308.

[6] Ball, P. Levitating trains make a racket, *Nature*, 2004. https://doi.org/10.1038/news040405-8.

[7] Shi, Z., Guo, J.L., Su, W.F., Zhang, S.Y., Analysis of dynamic wind of sound barrier under high speed train, *Applied Mechanics and Materials*, 361-363, 2013, 1536-1542.

[8] Carassale, L., Marrè Brunenghi, M., Dynamic response of trackside structures due to the aerodynamic effects produced by passing trains, *Journal of Wind Engineering and Industrial Aerodynamics*, 123, 2013, 317–324.

[9] Lü, J., Zhang, J., Liao, J., Hu, W., Tu, Y., Response of noise barrier for existing railway bridges under impulsive pressure induced by high-speed train, *Xinan Jiaotong Daxue uebao/Journal of Southwest Jiaotong University*, 44(4), 2009, 547-551.

[10] Lachinger, S., Reiterer, M., Kari, H., Comparison of calculation methods for aerodynamic impact on noise barriers along high speed rail lines, *11th World Congress on Rail Research*, Milan, Italy, 2016.

[11] Vittozzi, A., Silvestri, G., Genca, L., Basili, M., Fluid dynamic interaction between train and noise barriers on High-Speed-Lines, *Procedia Engineering,* 199, 2017, 290-295.

[12] Den Hartog, J.P., *Mechanical Vibrations*, McGraw-Hill, NewYork, 1934.

[13] Casciati, F., Giuliano, F., Performance of multi-TMD in the towers of suspension bridges, *Journal of Vibration and Control*, 15(6), 2009, 821-847.

[14] Chung, L.L., Wu, L.Y., Yang, C.S.W., Lien, K.H., Lin, M.C., Huang H.H., Optimal design formulas for viscous tuned mass dampers in wind-excited structures, *Structural Control and Health Monitoring*, 20(3), 2013, 320-336.

[15] Pietrosanti, D., De Angelis, M., Basili, M., Optimal design and performance evaluation of systems with Tuned Mass Damper Inerter (TMDI), *Earthquake Engineering and Structural Dynamics*, 46(8), 2017, 1367-1388.

[16] Barredo, E., Mendoza Larios, J.G., Mayén, J., Flores-Hernandez, A.A., Colín, J., Arias Montiel, M., Optimal design for high-performance passive dynamic vibration absorbers under random vibration, *Engineering Structures*, 195, 2019, 469-489.

[17] Warburton, G.B., Ayorinde, E.O., Optimum Absorber Parameters for Simple Systems, *Earthquake Engineering & Structural Dynamics*, 8, 1980, 197-217.

[18] Nishihara, O., Asami, T., Closed-form solutions to the exact optimizations of dynamic vibration absorbers minimizations of the maximum amplitude magnification factors, *Journal of Vibration and Acoustics*, 124(4), 2002, 576-582.

[19] Fujino, Y., Abe, M., Design Formulas for Tuned Mass Dampers Based on a Perturbation Technique, *Earthquake Engineering and Structural Dynamics*, 22, 1993, 833-854.

[20] Tubino, F., Piccardo, G., Tuned Mass Damper optimization for the mitigation of human-induced vibrations of pedestrian bridges, *Meccanica*, 50(3), 2015, 809-824.

[21] Roberson, R.E., Synthesis of a Nonlinear Dynamic Vibration Absorber, *Journal of the Franklin Institute*, 254, 1952, 205-220.

[22] Arnold, F., Steady state behaviour of systems provided with nonlinear dynamic vibration absorber, *Journal of Applied Mechanics*, 22, 1955, 487-492.

[23] Shaw, J., Shaw, S.W., Haddow, A.G., On the response of the non-linear vibration absorber, *International Journal of Non-Linear Mechanics*, 24, 1989, 281-293.

[24] Vakakis, A.F., Gendelman, O., Energy pumping in nonlinear mechanical oscillators II Resonance capture, *Journal of Applied Mechanics*, 68, 2001, 42-48.

[25] Kerschen, G., Lee, Y.S., Vakakis, A.F., McFarland, D.M., Bergman, L.A., Irreversible passive energy transfer in coupled oscillators with essential nonlinearity, *SIAM Journal of Applied Mathematics*, 66(2), 2005, 648-679.

[26] Vakakis, A.F., Gendelman, O.V., Bergman, L.A., Mcfarland, D.M., Kerschen, G., Lee, Y.S., *Nonlinear Targeted Energy Transfer in Mechanical and Structural Systems*. Springer, New York, 2008.

[27] Casini, P., Vestroni, F., Nonlinear resonances of hysteretic oscillators, *Acta Mechanica*, 229, 2018, 939-952.

[28] Vestroni, F., Casini, P., Mitigation of structural vibrations by hysteretic oscillators in internal resonance, *Nonlinear Dynamics*, 99, 2020, 505-518.

[29] Alexander, N.A., Schilder, F., Exploring the performance of a nonlinear tuned mass damper, *Journal of Sound and Vibration*, 319, 2009, 445-462.

[30] Luongo, A., Zulli, D., Dynamic analysis of externally excited nes-controlled systems via a mixed multiple scale/harmonic balance algorithm, *Nonlinear Dynamics*, 70(3), 2012, 2049-2061.

[31] Gourc, E., Michon, G., Seguy, S., Berlioz, A., Targeted energy transfer under harmonic forcing with a vibroimpact nonlinear energy sink: analytical and experimental developments, *Journal of Vibration and Acoustics*, 137(3), 2015, 031008.

[32] Habib, G., Romeo, F., The tuned bistable nonlinear energy sink, *Nonlinear Dynamics*, 89(1), 2017, 179-196.

[33] Shui, X., Wang, S., Investigation on a mechanical vibration absorber with tunable piecewise-linear stiffness, *Mechanical Systems and Signal Processing*, 100, 2018, 330-343.

[34] Gatti, G., Fundamental insight on the performance of a nonlinear tuned mass damper, *Meccanica*, 53, 2018, 111-123.

[35] Habib, G., Kadar, F., Papp, B., Impulsive vibration mitigation through a nonlinear tuned vibration absorber, *Nonlinear Dynamics*, 98(3), 2019, 2115-2130.

[36] Huang, Z., Hua, X., Chen, Z., Niu, H., Optimal design of TVMD with linear and nonlinear viscous damping for SDOF systems subjected to harmonic excitation, *Structural Control and Health Monitoring*, 26(10), 2019, e2413.

[37] Roy, A., Zhang, Z., Ghosh, A., Basu, B., On the nonlinear performance of a tuned sloshing damper under small amplitude excitation, *Journal of Vibration and Control*, 25(21-22), 2019, 2695-2705.

[38] Rustighi, E., Brennan, M.J., Mace, B.R., A shape memory alloy adaptive tuned vibration absorber: design and implementation, *Smart Materials and Structures*, 14, 2005, 19-28.

[39] Laxalde, D., Thouverez, F., Sinou, J.-J., Dynamics of a linear oscillator connected to a small strongly non-linear hysteretic absorber, *International Journal of Non-Linear Mechanics*, 41, 2006, 969-978.

[40] Carpineto, N., Lacarbonara, W., Vestroni, F., Hysteretic tuned mass dampers for structural vibration mitigation, *Journal of Sound and Vibration*, 333(5), 2014, 1302-1318.

[41] Barbieri, N., Barbieri, R., da Silva, R.A., Marcos José Mannala, M.J., Barbieri, L., Nonlinear dynamic analysis of wire-rope isolator and Stockbridge damper, *Nonlinear Dynamics*, 86, 2016, 501-512.

[42] Carboni, B., Lacarbonara, W., Nonlinear dynamic characterization of a new hysteretic device: experiments and computations, *Nonlinear Dynamics*, 83, 2016, 23-39.

[43] Casalotti, A., Lacarbonara, W., Tailoring of pinched hysteresis for nonlinear vibration absorption via asymptotic analysis, *International Journal of Non-linear Mechanics*, 94, 2016, 59-71.

[44] Piccirillo, V., Balthazar, J. M., Tusset, A. M., Bernardini, D., Rega, G., Application of a Shape Memory Absorber in Vibration Suppression, *Applied Mechanics and Materials*, 849, 2016, 27-35.

[45] Tang, B., Brennan, M.J., Gatti, G., Ferguson, N.S., Experimental characterization of a nonlinear vibration absorber using free vibration, *Journal of Sound and Vibration*, 367, 2016, 159-169.

[46] Basili, M., Casini, P., Morelli, L., Vestroni, F., A hysteretic absorber to mitigate vibrations of train noise barriers, *Journal of Physics: Conference Series*, 1264, 2019, 012033.

[47] Bouc, R., Forced vibrations of mechanical systems with hysteresis, *Proceedings of the Fourth Conference on Non-Linear Oscillations*, Prague, 1967.

[48] Wen, Y.K., Method of random vibration of hysteretic systems, *ASCE Journal of Engineering Mechanics*, 102(2), 1976, 249-263.

ORCID iD

Michela Basili https://orcid.org/0000-0001-6591-2738
Paolo Casini https://orcid.org/0000-0002-7308-4845
Laura Morelli https://orcid.org/0000-0002-1770-5862
Fabrizio Vestroni https://orcid.org/0000-0001-9299-0678